
CycleGAN, a Master of Steganography

Casey Chu
 Stanford University
 caseychu@stanford.edu

Andrey Zhmoginov
 Google Inc.
 azhmogin@google.com

Mark Sandler
 Google Inc.
 sandler@google.com

Abstract

CycleGAN is one of the latest successful approaches to learn a correspondence between two image distributions. In a series of experiments, we demonstrate an intriguing property of the model: CycleGAN learns to “hide” information about a source image inside the generated image in nearly imperceptible, high-frequency noise. This trick ensures that the complementary generator can recover the original sample and thus satisfy the cyclic consistency requirement, but the generated image remains realistic. We connect this phenomenon with adversarial attacks by viewing CycleGAN’s training procedure as training a generator of adversarial examples, thereby showing that adversarial attacks are not limited to classifiers but also may target generative models.

1 Introduction

Image-to-image translation is the task of taking an image from one class of images and rendering it in the style of another class. One famous example is artistic style transfer, pioneered by Gatys et al. [2015], which is the task of rendering a photograph in the style of a famous painter.

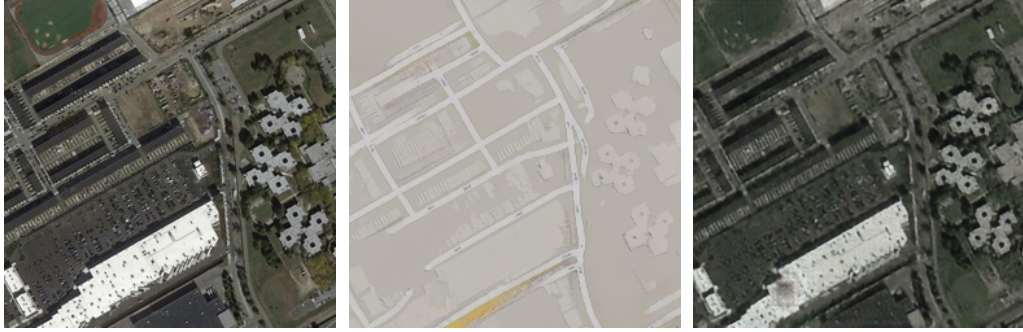
One recent technique for image-to-image translation has been CycleGAN [Zhu et al., 2017]. The CycleGAN architecture works by training two maps $F : X \rightarrow Y$ and $G : Y \rightarrow X$ in parallel with the goal of satisfying the following conditions

1. $Fx \sim p(y)$ for $x \sim p(x)$, and $Gy \sim p(x)$ for $y \sim p(y)$;
2. $GFx = x$ for all $x \in X$ and $FGy = y$ for all $y \in Y$,

where $p(x)$ and $p(y)$ describe the distributions of two domains of images X and Y . The second condition is called the *cyclic consistency loss*. For our experiments, we trained a CycleGAN model on a “maps” dataset consisting of approximately 1,000 aerial photographs X and 1,000 maps Y . The model trained for 500 epochs produced two maps $F : X \rightarrow Y$ and $G : Y \rightarrow X$ that generated realistic samples from these image domains.

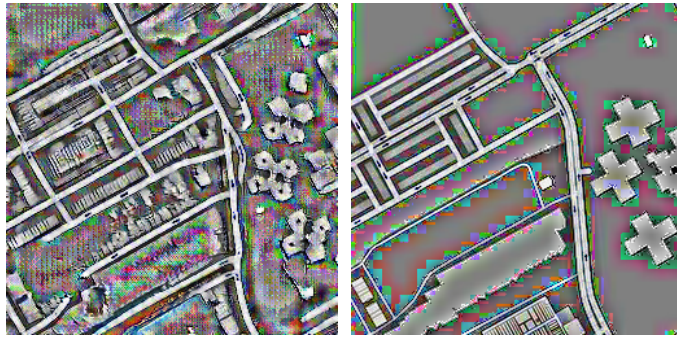
2 Hidden Information

We begin with a curious observation, illustrated in Figure 1. First, take an aerial photograph x that was unseen by the network at training time. Since the network was trained to minimize the cyclic consistency loss, one would expect that $x \approx GFx$ and indeed the two images turn out to be nearly identical. However, upon closer inspection, it becomes apparent that there are many details present in both the original aerial photograph x and the aerial reconstruction GFx that are not visible in the intermediate map Fx . For example, the pattern of black dots on the white roof in x is perfectly reconstructed, even though in the map, that area appears solidly gray. How does the network know



(a) Aerial photograph: x . (b) Generated map: Fx . (c) Aerial reconstruction: GFx .

Figure 1: Details in x are reconstructed in GFx , despite not appearing in the intermediate map Fx .



(a) Generated map. (b) Training map, for comparison.

Figure 2: Maps with details amplified by adaptive histogram equalization. Information is present in the generated map even in regions that appear empty to the naked eye.

how to reconstruct the dots so precisely? We observe this phenomenon with nearly every aerial photograph passed into the network, as well as when CycleGAN is trained on datasets other than maps.

We claim that CycleGAN is learning an encoding scheme in which it “hides” information about the aerial photograph x within the generated map Fx . This strategy is not as surprising as it seems at first glance, since it is impossible for a CycleGAN model to learn a perfect one-to-one correspondence between aerial photographs and maps, when a single map can correspond to a vast number of aerial photos, differing for example in rooftop color or tree location.

It may be possible to directly see where CycleGAN may be encoding this hidden information. When we zoom into an apparently solid region of the generated map, we in fact find a surprising amount of variation. We amplify this variation using an image processing technique called adaptive histogram equalization, which enhances contrast in a local neighborhood of each pixel, and present the results in Figure 2. For comparison, we apply the same transformation to a ground truth training map. We see that there does appear to be an extra, high-frequency signal in the generated map. We investigate the nature of this encoding scheme in the following sections.

3 Sensitivity to Corruption

In this section, we corrupt the generated map with noise and study how the aerial reconstruction changes, in order to characterize the nature of the encoding scheme. Specifically, let us define

$$V \equiv \mathbb{E}_{x \sim p(x), z \sim p(z)} \|G(Fx + z) - GFx\|, \quad (1)$$

where $p(x)$ is the true aerial distribution and $p(z)$ is a noise distribution. V measures how different the aerial reconstruction is when noise is added. We are interested in how V depends on the noise distribution $p(z)$, which in our experiments we chose to be Gaussian noise with standard deviation ϵ and spatial correlation σ .

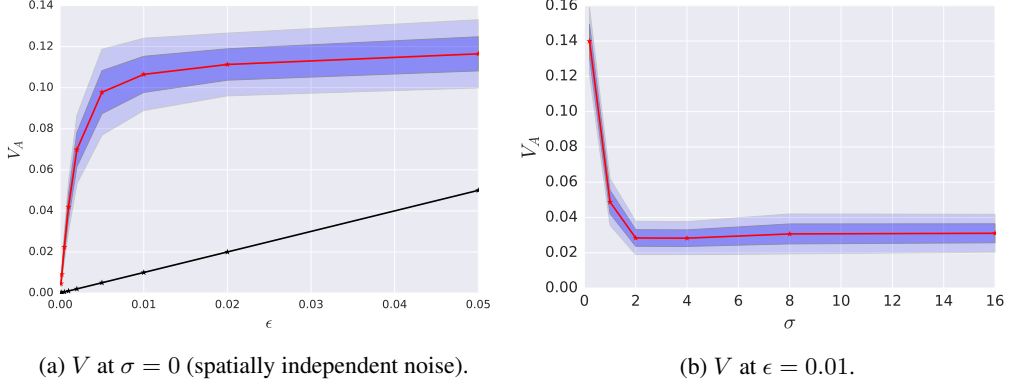


Figure 3: Sensitivity of G to noise as the amplitude ϵ and spatial correlation σ of the noise varies. In (a), $V = \epsilon$ is plotted for reference.



Figure 4: The information encoding is surprisingly non-local.

Figure 3 depicts how V behaves as a function of ϵ and σ . We approximated the expectation by averaging over 50 aerial photographs. We found that V attains nearly its maximum value as soon as $\epsilon \geq 3/256 \approx 0.01$, which corresponds to only 3 levels when the image is quantized by 8-bit integers. Thus an imperceptible modification of the map image can lead to major changes in the reconstructed aerial photograph. In fact, we found that simply encoding the generated map Fx with lossy JPEG compression destroyed the reconstruction. We also found that V quickly decays to its minimum value as soon as $\sigma \geq 2$, indicating that the information is fairly robust to low-frequency content, indeed such as the map itself. This suggests that the majority of information about the source photograph is stored in a high-frequency, low-amplitude signal within the generated map.

While G is quite sensitive to noise added to a map Fx , we show that G is well-behaved when a perturbation Δ created by F is added to Fx . Towards this end, we manually create two aerial images x' and x'' by editing a tree onto a grass field in x in two different locations; we then study the differences in the generated map $\Delta' = Fx' - Fx$ and $\Delta'' = Fx'' - Fx$. (Interestingly, the change Δ' is not localized around the added tree but extends far beyond this region, as shown in Figure 4.) We find that the reconstruction $G(Fx + \Delta' + \Delta'')$ contains both trees added in x' and x'' and does not contain any unexpected artifacts. This may indicate that the encodings Δ' and Δ'' are small enough that they operate in the linear regime of G , where

$$G(Fx + \Delta' + \Delta'') = GFx + dG\Delta' + dG\Delta'' + O(\Delta^2), \quad (2)$$

so that addition of perturbations in the map corresponds to independent addition of features in the generated aerial image. Indeed, we verified numerically that $G(Fx + \varepsilon\Delta')$ and $G(Fx + \varepsilon\Delta'')$ are approximately linear with respect to ε . Finally, we note that if Δ' is added to an entirely different image, the generated aerial image does not necessarily contain a tree and sometimes contains artifacts.



(a) Source map: y_0 . (b) Crafted map: y^* . (c) Difference: $y^* - y_0$. (d) Reconstruction: Gy^* .

Figure 5: Generation of a single target aerial photo x^* from two arbitrary maps y_0 . Note that (c) is amplified for visibility.

4 Information Hiding as an Adversarial Attack

In this section, we demonstrate that G has the ability to produce *any* desired aerial image from a specially crafted map y^* . Specifically, we solve the optimization problem

$$y^* = \arg \min_y ||Gy - x^*||, \quad (3)$$

where x^* is a target aerial image, starting with an initial map y_0 . This is similar to an adversarial attack [Szegedy et al., 2013] on G , where we are constructing an input y that forces G to produce a desired image. We optimize this objective using gradient descent and present the results in Figure 5. We find that the addition of a low-amplitude signal to virtually any initial map y_0 is sufficient to produce a given aerial image, and the specially crafted map y^* is visually indistinguishable from the original map y_0 .

In this light, we may think of the CycleGAN training procedure as mounting an adversarial attack on G , by optimizing a generator F to generate adversarial maps that force G to produce a desired image. Since we have demonstrated that it is possible to generate these adversarial maps using gradient descent; it follows that the training procedure will also push F to generate these adversarial maps. We also observe that the magnitude of the difference $y^* - y_0$ necessary to generate a convincing adversarial example by Equation 3 decreases as the CycleGAN model trains, indicating a degree of cooperation in G to support these adversarial maps.

5 Discussion

CycleGAN is designed to find a correspondence between two distinct probability distributions on domains X and Y . If X and Y are quite different, it may not be easy or possible to find a one-to-one mapping between them. CycleGAN is still successful at learning the mappings, but we demonstrated that it tends to “hide” at least some of the information about the input sample in a low-amplitude, high-frequency signal added to the output image. This makes the network output look realistic, while also allowing the complementary transformation to recover the original sample and thus satisfy cycle consistency requirement. This suggests that the CycleGAN objective may be in some sense too easy; instead of embedding information about the source image into semantic elements of the generated image, the model learns to cheat by encoding information into imperceptible elements. Future iterations of CycleGAN may require a more sophisticated cyclic consistency loss that prevents such simple tricks. Finally, we demonstrated that even generative models like CycleGAN may also be vulnerable to adversarial attacks, so some caution is required in applying them to problems of consequence.

Acknowledgments

We thank Jascha Sohl-Dickstein for his insightful comments.

References

G. K. Dziugaite, Z. Ghahramani, and D. M. Roy. A study of the effect of jpg compression on adversarial images. *arXiv preprint arXiv:1608.00853*, 2016.

L. A. Gatys, A. S. Ecker, and M. Bethge. A neural algorithm of artistic style. *arXiv preprint arXiv:1508.06576*, 2015.

I. Goodfellow, J. Pouget-Abadie, M. Mirza, B. Xu, D. Warde-Farley, S. Ozair, A. Courville, and Y. Bengio. Generative adversarial nets. In *Advances in neural information processing systems*, pages 2672–2680, 2014a.

I. J. Goodfellow, J. Shlens, and C. Szegedy. Explaining and harnessing adversarial examples. *arXiv preprint arXiv:1412.6572*, 2014b.

J. Kos, I. Fischer, and D. Song. Adversarial examples for generative models. *arXiv preprint arXiv:1702.06832*, 2017.

H. Shi, J. Dong, W. Wang, Y. Qian, and X. Zhang. Ssgan: Secure steganography based on generative adversarial networks. *arXiv preprint arXiv:1707.01613*, 2017.

C. Szegedy, W. Zaremba, I. Sutskever, J. Bruna, D. Erhan, I. Goodfellow, and R. Fergus. Intriguing properties of neural networks. *arXiv preprint arXiv:1312.6199*, 2013.

P. Tabacof, J. Tavares, and E. Valle. Adversarial images for variational autoencoders. *arXiv preprint arXiv:1612.00155*, 2016.

D. Volkhonskiy, I. Nazarov, B. Borisenko, and E. Burnaev. Steganographic generative adversarial networks. *arXiv preprint arXiv:1703.05502*, 2017.

J.-Y. Zhu, T. Park, P. Isola, and A. A. Efros. Unpaired image-to-image translation using cycle-consistent adversarial networks. *arXiv preprint arXiv:1703.10593*, 2017.